Astronomical and Astrophysical Transactions (*AApTr*), 2018, Vol. 30, Issue 3, pp. 315–322,
ISSN 1055-6796, Photocopying permitted by license only, ©Cambridge Scientific Publishers

Lithium, sodium and potassium resonance lines pressure broadened by helium atoms

R. Beuc[1,*], G. Peach[2], M. Movre[1], B. Horvatić[1]

[1] *Institute of Physics, Bijenička cesta 46, HR-10000 Zagreb, Croatia*
[2] *University College London, London WC1E 6BT, UK*

Received 20 June, 2016

The resonance lines of alkali-metal atoms, broadened by collisions with helium atoms, are prominent features in the spectra of brown dwarfs. We carried out calculations of the emission and absorption spectra in the far red and blue wings of the first resonant doublets of lithium, sodium and potassium perturbed by helium atoms, for temperatures from 500 to 3000 K. For our calculation we used carefully constructed electronic adiabatic potential energy curves and electronic transition dipole moments of Li–He, Na–He and K–He molecules. In the computation of the emission and absorption coefficients, we used the fully quantum-mechanical calculation, based on the Fourier grid Hamiltonian method. The obtained absorption and emission spectra are compared with previous theoretical calculations.

Keywords: Molecular data – line: profiles – stars: brown dwarfs

1 Intoduction

Broadening of alkali-metal resonance lines in the presence of perturbing atoms and molecules has been extensively studied over several decades. Experimental methods such as laser-induced fluorescence, emission and absorption spectroscopy, were used to study the properties of the atom–perturber interactions in the context of various applications such as the modelling of high-pressure alkali lamps and optical diagnostics of gas temperature and abundance. Especially intensive have been the experimental investigations of alkali-metal atoms' line broadening with noble gas atoms (Lalos et al. 1962, Scheps et al. 1975, York et al. 1975, Chung et al. 2002, Shindo et al. 2007).

In the last two decades the pressure broadening of alkali-metal resonance lines has gained a new importance in astrophysical research as well. It has been found that prominent features in the spectra of brown dwarfs and extrasolar giant planets might be attributed to the resonance lines of the alkali-metal atoms broadened by collisions with the ambient hydrogen molecules and helium atoms (Burrows et al.

*Email: beuc@ifs.hr

2003, Sharp et al. 2007). Alkali-metal resonance lines shape the optical spectrum from the ultraviolet to the near-infrared spectral range. Detailed knowledge of the line profiles as functions of temperature and pressure can be obtained from both the fully quantum-mechanical and semiclassical calculations using accurate molecular potential energy curves and dipole transition moments for the alkali–perturber system. These enable the interpretations of the measured spectra, which yield information on the temperatures, densities, albedos and compositions of the stellar atmospheres.

Pressure broadening of light alkali (Li, Na, K) lines by He atoms has a remarkable importance. Impact broadening of light alkali lines was studied quantum-mechanically in Peach et al. (2006), Mullamphy et al. (2007), Allard et al. (2007). Far wings of light alkali lines broadened by helium were theoretically analyzed in Zhu et al. (2005), Alioua et al. (2008), Zhu et al. (2006), Babb (2010), Allard et al. (2014).

2 Calculations and results

Molecular-structure calculations of A–He molecules (where A = Li, Na, K) have been performed neglecting the spin–orbit interaction. The A–He molecule is treated in a three-body model, as an A^+ ion plus a valence electron and a He atom represented by a polarizable atomic core (Peach 1982, Mullamphy et al. 2007). The electron–helium atom and electron–alkali ion interactions are represented by model potentials. The core–core interaction is also calculated using a three-body model composed of A^+ and He^+ cores plus one electron. The molecular electronic potentials $V(R)$ and transition dipole moments $D(R)$ were obtained over a large range of interatomic distances, allowing a good description of the spectral line core.

Potential energy curves for the lowest three electronic states of A–He molecules are shown in Fig. 1. The zero of energy corresponds to the asymptotic energy $V(R \to \infty)$ of the ground $X^2\Sigma^+$ state. Potential curves of the lowest electronic states have qualitatively the same shape for all three dimers. The ground $X^2\Sigma^+$ state potential curves are predominantly repulsive, exhibiting just a shallow well at large interatomic distances (R_e = 11.8 a$_0$, D_e = 0.0015 cm^{-1}; R_e =12.2 a$_0$, D_e = 1.4 cm^{-1}; and R_e = 13.8 a$_0$, D_e =1.2 cm^{-1}, respectively). The excited $B^2\Sigma^+$ state potential curves are of a similar character: R_e = 16.5 a$_0$, D_e = 0.58 cm^{-1}; R_e = 18.7a$_0$, D_e = 0.41 cm^{-1}; and R_e = 20.5 a$_0$, D_e = 0.34 cm^{-1}, respectively. On the other hand, the excited $A^2\Pi$ states of Li–He, Na–He, and K–He molecules have the potential well at small interatomic distances (R_e = 3.3 a$_0$, D_e = 1060.2 cm^{-1}; R_e = 4.4 a$_0$, D_e = 422.8 cm^{-1}; and R_e = 6.2 a$_0$, D_e = 129.2 cm^{-1}, respectively). Difference potentials for the transitions between the ground and the lowest excited electronic states and the corresponding transition dipole moments, shown in Fig. 1, also have qualitatively the same shape for all three dimers.

To the thermally averaged absorption coefficient contribute all transitions from rovibrational states of a lower electronic state Λ'' to rovibrational states of the upper electronic state Λ'. In each electronic state Λ there is a finite number of bound and quasibound states with energies $E_{v,J,\Lambda}$ and the unity-normalized wave functions $\Phi_{v,J,\Lambda}(R)$ (ν is the vibrational, J the rotational quantum number), and continuum free rovibrational states with asymptotic energies ϵ and energy-normalized wave functions $\Phi_{\epsilon,J,\Lambda}(R)$.

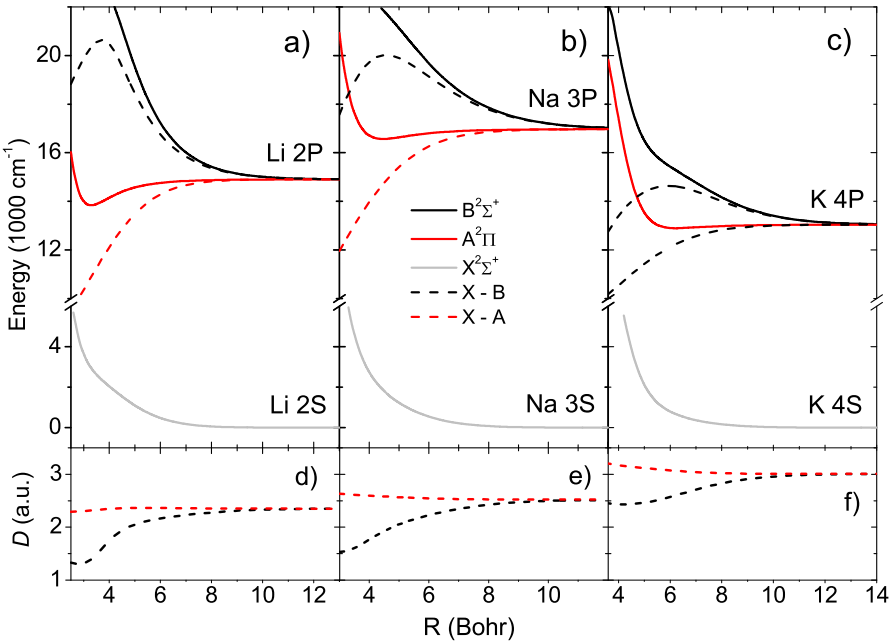


Figure 1 Potential energy curves for the lowest electronic states of an A–He molecule: a) Li–He, b) Na–He, c) K–He. Dashed lines represent the difference potentials for the X–A and X–B transitions. The absolute values of electronic dipole moments for these transitions are shown in d), e), and f) for Li–He, Na–He and K–He molecules, respectively.

When the Fourier-grid-Hamiltonian method (FGH) is applied (Colbert and Miller 1992), rovibrational wave functions are represented on a finite number of uniformly spaced grid points R_i $(i = 1,\ldots N)$, $\Phi_{v(\epsilon),J,\Lambda}(R) \to \Phi_{v,J,\Lambda}(R_i)$. The Hamiltonian is represented on the grid by an $N \times N$ matrix

$$H(\Lambda,J)_{i,j} = \begin{pmatrix} V_\Lambda(R_i) + \dfrac{\hbar^2}{2\mu}\dfrac{J(J+1)+\Lambda^2}{R_i^2} + \dfrac{\hbar^2}{2\mu\Delta R^2}\dfrac{2\pi^2 i^2 - 3}{6i^2} & i = j \\ \dfrac{\hbar^2}{2\mu\Delta R^2}\dfrac{8ij(-1)^{i-j}}{(i^2-j^2)^2} & i \neq j \end{pmatrix}, \quad (1)$$

where $V_\Lambda(R)$ is the adiabatic potential of the electronic state, Λ the electronic angular moment of this state, ΔR the distance between the neighbouring grid points, and μ the reduced mass of the molecule.

The infinite set of rovibrational states is represented on the grid by a finite set of states whose energies $E_{v,J,\Lambda}$ and wave functions $\Phi_{v,J,\Lambda}$ $(\nu = 1,\ldots N)$ are the eigenvalues and eigenvectors of the above matrix H. The continuum of free states is represented by a discrete set of unity-normalized wave functions having a node at the outer grid boundary $R_N = N \cdot \Delta R$.

In the case of local thermodynamic equilibrium (LTE), in the binary (low-pressure) approximation, and assuming the Q-branch approximation $(\Delta J = 0)$, the reduced

absorption coefficient for temperature T and frequency ν has the form (Beuc et al. 2012, Chung et al. 2001):

$$k(\nu,T) = \\ = w\frac{h^2\nu}{c}\left(\frac{2\pi}{k_BT}\right)^{\frac{3}{2}}\sum_{J}^{J_{\max}}(2J+1)\sum_{\nu'',\nu'}^{N,N}e^{-\frac{E_{v'',J,\Lambda''}}{k_BT}} \\ \times\left|\langle\Phi_{v'},J,\Lambda''\left|D(R)\right|\Phi_{v',J,\Lambda'}\rangle\right|^2 g(\nu-\nu_{\rm tr}), \tag{2}$$

where w is a statistical factor (1/3 for X–B, 2/3 for X–A transitions), $J_{\max}$ is the largest J value, $g(\nu)$ is the "instrumental" profile, and $\nu_{\rm tr} = \left(E_{v',J,\Lambda'} - E_{v'',J,\Lambda''}\right)/h$ are the transition frequencies.

The parameters for the calculation are estimated in the following way. Aiming to simulate the spectra for temperatures up to $T_{\max}$, we chose the local radial kinetic energy cut-off amounting to $E_N = 5k_BT_{\max}$. Taking $E_N = 10000$ cm^{-1}, our calculations are reliable for temperatures up to $T_{\max} = 3000$ K. The step size is given by $\Delta R = \pi\hbar/\sqrt{2\mu E_N}$. $J_{\max}$ was estimated according to $\hbar^2J_{\max}^2/2\mu R_J^2 \cong E_N$, with $R_J \leq R_N$, where $V_\Lambda(R_J)$ is close enough to the asymptotic energy $V_\Lambda(\infty)$. In our calculations we chose $R_J = 13,\ 14,\ 15\ a_0$ and get $J_{\max} = 288,\ 333,\ 343$ for Li–He, Na–He, K–He, respectively. Finally, we chose $N = 500$ grid points and we got $R_N = 76,\ 66,\ 64\ a_0$ for Li–He, Na–He, K–He, respectively.

There is a large number $J_{\max} \times N^2$ of transitions contributing to the spectrum. Therefore we took into account only the transitions which satisfy the conditions $\nu_{\min} \leq \nu_{\rm tr} \leq \nu_{\max}$ and $|\langle\Phi_{v'',J,\Lambda''}|\Phi_{v',J,\Lambda'}\rangle| \leq 0.0001$.

We calculated 8–9 million matrix elements using about 5–6 minutes of computer time, for each molecule. To evaluate the absorption coefficient for a given temperature, the spectrum was collected in bins of the size $\Delta\nu/c = 2$ cm^{-1}, and smoothed with a triangle profile (FWHM 10 cm^{-1}), consuming 20–25 seconds of computer time.

In the neighbourhood of the atomic transition ν_0, for an optically thick medium, the emission coefficient is simply related to the reduced absorption coefficient (Horvatić et al. 2015) as

$$\varepsilon(\nu,T) = \frac{8\pi\nu^2}{c^2}e^{-\frac{h(\nu-\nu_0)}{k_BT}}k(\nu,T). \tag{3}$$

The reduced absorption coefficients (the first row of Fig. 2) and emission coefficients (the second row of Fig. 2) of A–He dimers exhibit the same qualitative behavior. The X–B transition, comprising only free-free rovibrational transitions, forms the blue wing of the atomic line. On the short-wavelength side, the wing terminates with a blue satellite band which is a consequence of an extremum in the X–B transition difference potential curve. The X–A transition has a monotonic difference potential and both free–free and free–bound rovibrational transitions contribute to the formation of the red wing. In the spectral range where the Condon transitions are connected with the attractive well of the $A^2\Pi$ state, Stückelberg oscillations occur. These oscillations increase with temperature and with the depth of the potential well in the $A^2\Pi$ states of the A–He molecule.

The reduced absorption coefficient increases with temperature because the initial state is the repulsive $X^2\Sigma^+$ state. The emission coefficient of the blue wing also increases with temperature because the initial state of the transition is the repulsive

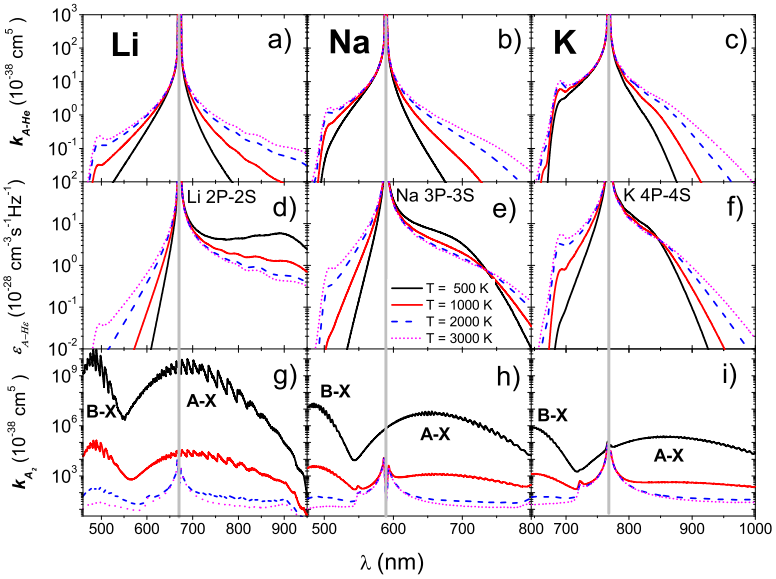


Figure 2 The first row (a, b, c) shows the reduced absorption coefficient of the far wings of Li, Na and K resonant doublets broadened by helium atoms for different temperatures, the second row (d, e, f) shows the corresponding emission coefficients, and the third row (g, h, i) shows the reduced absorption coefficient of alkali diatomic molecules (Li_2, Na_2, K_2). Vertical grey lines show the positions of resonant doublets.

$B^2\Sigma^+$ state. In the red wing the emission coefficient increases with temperature in the spectral range where Condon transitions are connected with the repulsive part of $A^2\Pi$, and decreases in the region where Condon transitions are connected with the attractive part of this state. As a consequence, there is a broad plateau or satellite in the red wing for low temperatures, connected with the minimum of the $A^2\Pi$ potential well.

Our calculations are in good agreement with previous theoretical and experimental results. There is a small difference in satellite positions and intensities due to the difference in molecular potential curves applied.

In the case of the Li–He molecule we obtain the position of the blue satellite at 496.8 nm and the low-temperature red-wing emission plateau at 892 nm. Lalos et al. (1962) in the emission measurement in a ballistic compressor (T = 3600–6200 K, P = 500–2000 Torr) observed the Li–He band near 530 nm. Scheps et al. (1975) in the fluorescence emission spectrum (T = 600 K, P = 600 Torr) observed the red wing broad plateau which extends to 900 nm. Zhu et al. (2005) in a theoretical study report a blue satellite at 536 nm and a red satellite at 870 nm. Allard et al. (2014) get the position of the blue wing satellite at 526 nm using potential curves of Dell'Angelo (2012) and at 500 nm for the potential curves of Pascale (1983).

For the Na–He molecule we obtain the position of the blue satellite at 508 nm. York et al. (1975) analyzed experimentally the red wing emission spectra (T = 403 K, P = 608 Torr). Chung et al. (2002) in the absorption measurement (T = 850–910 K) observed a weak satellite peak at 530 nm. By the fully quantum mechanical

treatment Zhu et al. (2006) predict the position of the satellite band near 532 nm, and Alioua et al. (2008) at 528 nm.

In the case of K–He our calculation gives the blue satellite in the absorption and emission spectra at 692.5 nm, while Zhu et al. (2006) find a satellite near 708 nm. Baab et al. (2010) report the absorption measurement at $P = 170$ and 430 Torr, where the blue satellite is observed near 710 nm.

3 Discussion and conclusions

For the light transmission through a uniform layer of alkali and helium vapour (of thickness L, temperature T, alkali number density N_A, helium number density N_{He}) the optical depth is given by

$$\varepsilon(T,\nu) = LN_{He}N_A k_{A-He}(T,\nu) + LN_A^2 k_{A_2}(T,\nu). \quad (4)$$

Using the quantum mechanical FGH method we calculated the reduced absorption coefficient for A_2 dimers in the temperature range of 500–3000 K, shown in the third row of Fig. 2. In the calculations we used the molecular potential data of Schmidt-Mink et al. (1985) for Li_2, Magnier (1993) for Na_2 and Yan & Meyer (unpublished) for K_2. The reduced absorption coefficient of an A_2 dimer decreases with temperature and is much larger than the A–He absorption coefficient because of the deep well of the ground-state potential. In order to observe the broadening of alkali lines by helium atoms, the partial A–He optical depth must be comparable to or larger than the partial depth of an alkali dimer contribution. This holds for higher temperatures and/or in the case where the number density of helium atoms is much larger than the alkali number density, what is satisfied in a stellar atmosphere.

In order to get a powerful tool for analyzing the atmospheres of brown stars, one needs precise molecular potential curves and transition dipole moments, a correct and time-efficient spectral simulation (we believe that our FGH method is one of such), and laboratory experimental verification in a large interval of temperatures and pressures. The last requirement is probably the hardest to achieve.

Acknowledgement We gratefully acknowledge the Croatian Science Foundation (HRZZ) funding this work through the research project No. 2753.

References

Alioua K., Bouledroua M., Allouche A. R., Aubert-Frécon M. 2008, J. Phys. B, 41, 175102

Allard N. F., Kielkopf J. F., Allard, F., 2007, Eur. Phys. J. D, 44, 507

Allard N. F., Nakayama A., Stienkemeier F., Kielkopf J. F., Guillon G., Viel A. 2014, In Advances in Space Research, Elsevier

Babb J. 2010, Harvard-Smithsonian, CfA Lab. Astro. Symposium

Beuc R., Movre M., Horvatić B. 2014, Eur. Phys. J. D, 68, 59

Burrows A., Volobuyev M. 2003, ApJ, 583, 985

Chung H.-K., Kirby K., Babb J. F. 2001, Phys. Rev. A, 63, 032516
Chung H.-K., Shurgalin M., Babb J. F. 2002, 16th ICSLS
Colbert D. T., Miller W. H. 1992, J. Chem. Phys., 96, 1982
Dell'Angelo D., Guillon G., Viel, A. 2012, J. Chem. Phys., 136, 114308
Horvatić B., Beuc R., Movre M. 2015, Eur. Phys. J. D, 69, 113
Lalos G. T., Hammond G. L. 1962, ApJ, 135, 616
Magnier S. 1993, PhD Thesis, Orsay, France: University of Paris XI
Mullamphy D. F. T., Peach G., Venturi V., Whittingham I. B., Gibson S. J. 2007, J. Phys. B, 40, 1141
Pascale J. 1983, Phys. Rev. A 28, 632
Peach G. 1982, Comments on Atomic and Molecular Physics, 11, 101
Scheps R., Ottinger C., York G., Gallagher A. 1975, J. Chem. Phys., 63, 2581
Schmidt-Mink I., Muller W., Meyer W. 1985, Chem. Phys., 92, 263
Sharp C. M., Burrows A. 2007, ApJ Suppl., 168, 140
Yan L., Meyer W., unpublished results
York G., Scheps R., Gallagher A. 1975, J. Chem. Phys., 63, 1052
Zhu C., Babb J. F., Dalgarno A. 2005, Phys. Rev. A, 71, 052710
Zhu C., Babb J. F., Dalgarno A. 2006, Phys. Rev. A, 73, 012506